On 3D structure of a circular cylinder wake

Václav Uruba[1,2,*], *Pavel* Procházka[1], and *Vladislav* Skála[1]

[1]Institute of Thermomechanics of the Czech Academy of Sciences, Dolejškova 5, Praha 8, CR
[2]University of West Bohemia, Faculty of Mechanical Engineering, Department of Power System Engineering, Universitní 8, Plzeň, CR

Abstract. The 3D structure of the wake behind a circular cylinder in a cross-flow is studied experimentally using stereo PIV technique, Reynolds number was around 5 thousands. The statistical characteristics along the cylinder axis are effectively constant and thus 2D, however instantaneous flow-field in the wake is fully 3D. Within the wake dynamical flow, the streamwise vortices and spots of streamwise velocity component pulsations are detected.

1 Introduction

Many types of flows in practice could be characterized by 2D boundary conditions very often. Typical example could be cross-flow around a prismatic body. In spite of inherent dynamical nature of the flow-field if turbulent, this case could be considered as a plane, 2D flow, invariant along the body (excluding the ends). Such a case is also mathematically modelled as a 2D flow as a rule, taking into account only a single cross-section, supposing the same flow picture for any other section along the body axis.

The case of circular cylinder in cross-flow is one from the family of so called canonical cases. We could find extensive information source on this case in available literature covering theoretical, experimental and numerical studies respectively. Most of available studies treat the prismatic cylinder as forced 2D case, thus no 3D structures are detected, of course. The 3D structure of the wake behind a body of 2D geometry has been already addressed in several papers, see e.g. in [1]. The paper [2] deals with the d'Alembert paradox (zero forces) for inviscid flow and shows that this paradox is due to forcing 2D stationary flow pattern, which represents one of the solutions of the Naiver-Stokes equations, however instable one. The other, stable solution is represented by 3D and non-stationary flow pattern. This complies with reality. Then, the adequate forces are generated even in the inviscid case and the d'Alembert paradox is thus resolved.

It is known that the real wake behind circular cylinder contains several types of flow patterns: steady, unsteady periodical and chaotic, some of them are 2D character, but most of them are 3D. The control parameter is Reynolds number defined using the incoming velocity, cylinder diameter and fluid kinematic viscosity. Description of the wake topology including its dynamics could be find in any good book on fluid mechanics, more information on the details are in numerous papers, see e.g. [3].

In the presented paper the 3D non-stationary structures in the wake are to be addressed.

2 Experimental setup

The experiments were carried out in the Laboratory of Turbulent Shear Flows in Institute of Thermomechanics of the Czech Academy of Sciences. The blow-down facility was used with open test section, cross-section was 250 x 250 mm^2. Quality of the flow was good, velocity regularity was within 1% of the outlet velocity U_e = 5 m/s, intensity of velocity fluctuation was less than 0.5% of it.

2.1 Physical model

The model of cylinder ϕ d = 15 mm was fixed on the contraction output flange in its axis, perpendicularly to the output flow, 250 mm of the cylinder length was placed in the flow. The situation including measuring device is depicted schematically in Fig. 1.

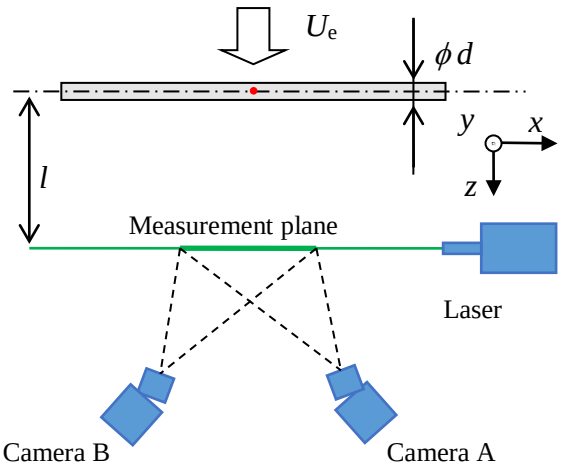

Fig. 1. Experimental setup.

* Corresponding author: uruba@it.cas.cz

© The Authors, published by EDP Sciences. This is an open access article distributed under the terms of the Creative Commons Attribution License 4.0 (http://creativecommons.org/licenses/by/4.0/).

The wake is studied in the distance $l = 8\ d$ (120 mm) behind the cylinder, the measurement plane is perpendicular to the incoming flow and parallel to the cylinder axis (shown in green in Fig. 1).

In Fig. 1 the Cartesian coordinate system is introduced with z axis parallel to the flow and x axis parallel to the cylinder axis. The origin is placed to the cylinder axis in the middle of the Field of View (hereinafter FoV) – the red dot in Fig. 1.

2.2 Experimental technique

The Stereo PIV time-resolved measuring technique was used to evaluate all three velocity component in the plane of measurement. The measuring apparatus is by Dantec company.

The laser (see Fig. 1) New Wave Pegasus, Nd:YLF double-head, was used to illuminate the particles. The used light was with wavelength of 527 nm, maximal frequency is 10 kHz, shot energy is 10 mJ (for 1 kHz) and corresponding power is 10 W per head. Two CMOS cameras NanoSense MKIII with Scheinpflug mounting of lenses were used (in Fig. 1 the "Camera A" and "Camera B") to capture the tracing particles distributed in the flow. Each camera has resolution of 1280 x 1024 pixels, maximal corresponding acquisition frequency is 512 double-snaps per second.

The data acquisition was controlled by the Dynamic Studio software. The calibration was performed using standard calibration target 100 x 100 mm. Precise positioning of the calibration target was performed by the stepper motor in five positions (-2, -1, 0, 1, 2 mm). The pinhole camera model was used for the pictures dewarping. The calibration error was approximately 0,2 pixels. 1600 double-snaps have been acquired with frequency 500 Hz, representing 3.2 s of the time record. The schematic view of stereo PIV layout is in Fig. 1.

The Safex generator of particles in the form of oil droplets, the mean diameter of the particles was 1 μm.

2.3 Analysis methods

First, the data is subjected to classical statistical analysis. The methods as calculation of mean values, variances and covariances are used.

To study the dynamical properties of the flow-field the Oscillation Pattern Decomposition method (OPD) was adopted resulting in series of OPD modes. Each OPD mode is characterized by its topology in complex form (consisting of real and imaginary parts), frequency and attenuation of the pseudo-periodic (oscillating) behaviour. Attenuation or amplitude decay is described by so called e-folding time τ_e representing the mean time period of the mode amplitude decay by "e". The other decay characteristic is dimensionless "periodicity" p which expresses the e-folding time in multiples of periods of the mode. The details on OPD method could be found in [4,5].

3 Results

All results are to be shown in dimensionless form. The geometric dimensions are expressed in multiples of the cylinder diameter d and the velocities in multiples of the inlet velocity U_e.

3.1. Mean values

The time-mean values of the acquired spatio-temporal data are to be shown in the form distributions within the plane of measurement. The measurement plane is located in the position $z = 8$, the cylinder axis in the dash-dot line $y = 0$ and projection of the cylinder contours are depicted as dashed lines $y = +\text{-}0.5$.

In Fig. 2 the mean velocity distribution is shown, the in-plane velocity vector components are represented by arrows, while the out-of-plane component W (in z direction) is represented by colour. The scale of the vectors is shown in left-bottom corner, showing the size of 0.1. The vector-lines of in-plane velocity vector components are added arbitrarily for better visibility of the vector-field.

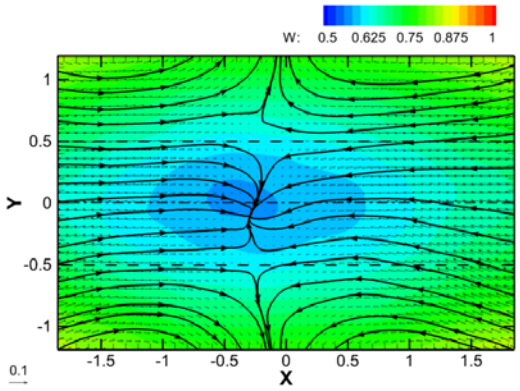

Fig. 2. Mean velocity distribution.

The minimum of the mean velocity is located just in the middle close to the coordinate's origin, forming a sink. In reality no sink could exist in the mean velocity field because of continuity condition. The weak sink in our case is a consequence of a view distortion by the cameras located on sides – see Fig. 1. The mean velocity distribution is close to 2D situation, independent on x. Minimum of the mean streamwise velocity component is located on the cylinder axis x. The spanwise mean velocity components are close to zero.

The Turbulent Kinetic Energy (hereinafter TKE) distribution is in Fig. 3. Maximum of the TKE is within the wake behind the cylinder body, close to the cylinder axis. The distribution is again close to 2D.

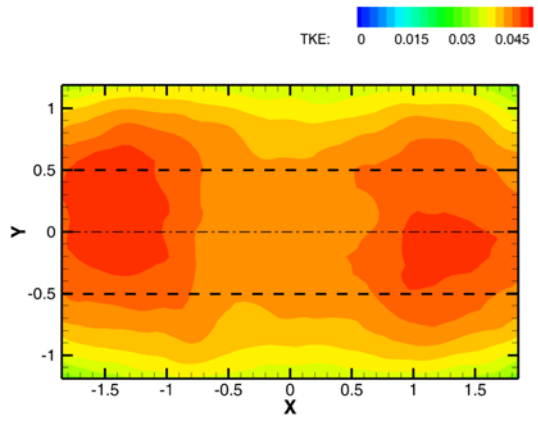

Fig. 3. TKE distribution.

All 3 correlation coefficients between individual velocity components have been evaluated, however only the correlation coefficient (VW) between streamwise and spanwise perpendicular to the cylinder axis velocity components contains important values, see Fig. 4. The rest two coefficients approaches zero in the whole region.

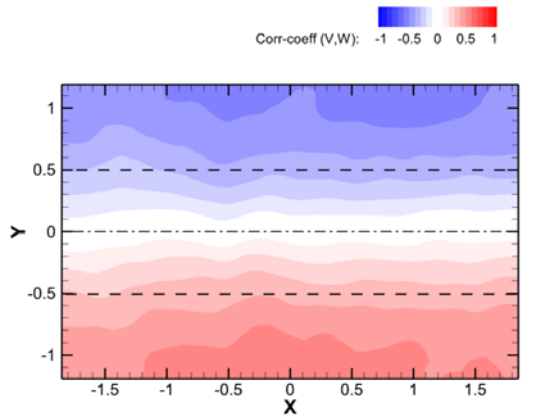

Fig. 4. (VW) correlation coefficient distribution.

This result show turbulence production in shear layers on above and below the cylinder location. Disproportion between the correlation coefficients indicates important anisotropy of the turbulence in the cylinder wake.

3.2 Dynamics

The OPD analysis has been performed on the acquired data. The numerical parameters of all evaluated OPD modes are shown in Table 1.

The OPD modes numbering is made according to their frequency in ascending order. 15 OPD modes have been evaluated.

The OPD modes could be divided into several groups. In Table 1 the dominant OPD mode with high periodicity value is marked by red colour. Blue colour means modes with periodicity about 0,2, green about 0,1 and white (no colour) are mode with very small periodicity values, less than 0,05.

Table 1. OPD modes.

No.	f [Hz]	τ_e [ms]	p [1]
1	0	0.126	0
2	0	0.796	0
3	0	0.506	0
4	0	0.358	0
5	5.14	0.565	0.029
6	5.72	0.283	0.016
7	9.27	0.372	0.035
8	13.17	0.333	0.044
9	17.24	0.516	0.089
10	23.54	0.412	0.097
11	27.12	0.311	0.084
12	35.16	0.583	0.205
13	43.19	0.431	0.186
14	45.36	3.664	1.662
15	62.25	0.461	0.287

Next, the OPD modes are represented graphically in the Frequency-Periodicity plane in Fig. 5 in the form of the spectrum.

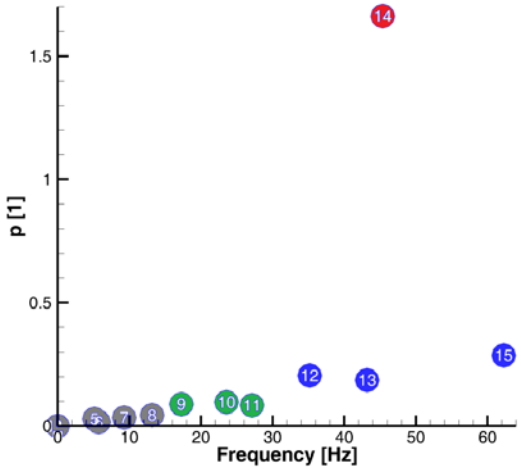

Fig. 5. OPD spectrum.

In Fig. 5 the OPD modes are distinguished by numbers and colours, similarly as in Table 1.

The topology of the OPD modes consists of real and imaginary parts representing the cyclostationary process in different phases shifted by $\pi/2$ from each other.

The dominant OPD mode 14 is characterized by very high periodicity and it is directly related to the vortex shedding process in the wake. It is described by parameters marked by red colour in Table 1. Real and imaginary parts of this OPD mode are shown in Figures 6 and 7 respectively.

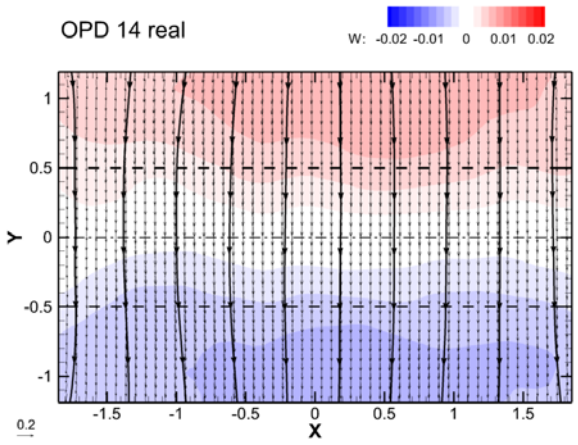

Fig. 6. Real part of the OPD mode 14 topology.

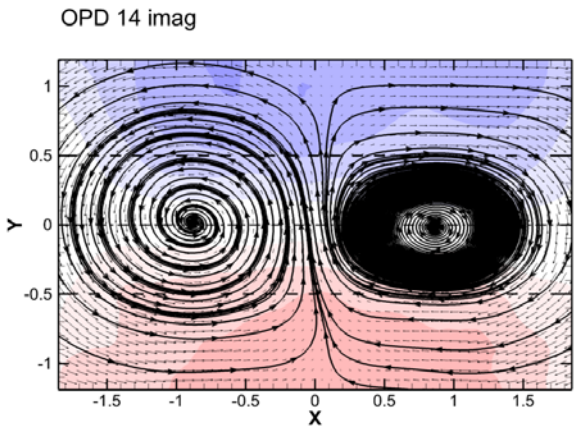

Fig. 7. Imaginary part of the OPD mode 14 topology.

The real part of the OPD mode is shown in Fig. 6 and documents 2D structure of the fluctuation flow-field. On the other hand the imaginary part in Fig. 7 and it contains a contra-rotating pair of streamwise vortices with spacing 2 cylinder diameters. The distribution of the *w* fluctuation velocity component is similar as for the real part but opposite.

The von Kármán vortex street dynamics have been studied in details in [6], where results of measurement in the plane parallel to the flow and perpendicular to the cylinder axis are shown.

The real part of its topology shows parallel flow in *y* direction transversal to both flow and cylinder axis. The streamwise velocity component forms shear region with the velocity amplitudes in the top and bottom of the FoV respectively. In the middle of the FoV, close to the cylinder axis, there is fluctuation close to zero.

The topology of the POD mode 14 suggests periodic appearance of the system contra-rotation streamwise vortices during one half of the period, then disappearing and reappearing again. This process is accompanied by pulsations of the flow in *y* direction and streamwise velocity component shear configuration.

Obviously, the OPD mode 14 is connected with the vortex-shedding process known as von Kármán Vortex Street. These vortices are oriented in *x* direction shedding alternatively from the cylinder sides with the same frequency as the OPD mode 14 and moving in streamwise direction. Existence of the OPD mode 14 suggests, that the von Kármán vortices are structured along the cylinder axis *x* containing streamwise vorticity.

Next, we are going to present the 3 OPD modes 12, 13, 15 with periodicity value around 0,2. The real and imaginary parts of the OPD mode 12 are shown in Figures 8 and 9. The mode is represented by alternation of single streamwise vortex and contra-rotating pair of streamwise vortices. The streamwise fluctuating velocity component forms spotty structures in the domain. All the involved structures are smaller and less regular than those in the case of dominant OPD mode 14, confirm Figures 6 and 7.

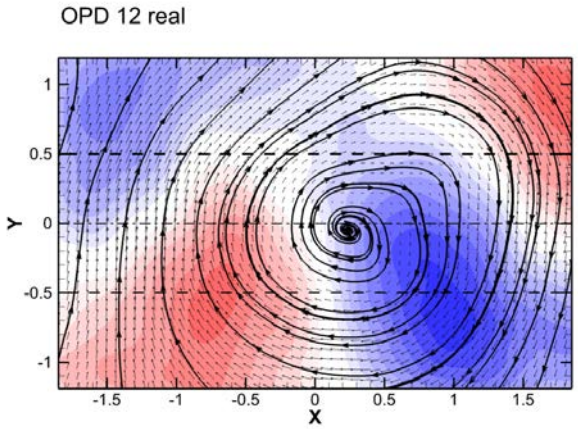

Fig. 8. Real part of the OPD mode 12 topology.

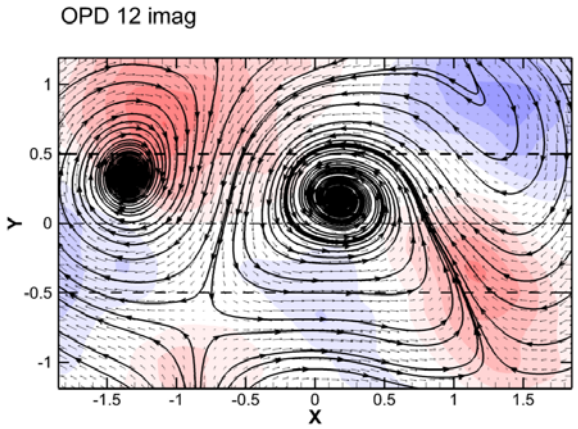

Fig. 9. Imaginary part of the OPD mode 12 topology.

The OPD modes 13 and 14 are quite similar to each other. The dominant structures are big amplitude positive and negative fluctuations of streamwise velocity component along the cylinder axis *x*. Only real parts of the OPD modes 13 and 14 are shown in Figures 10 and 11 respectively.

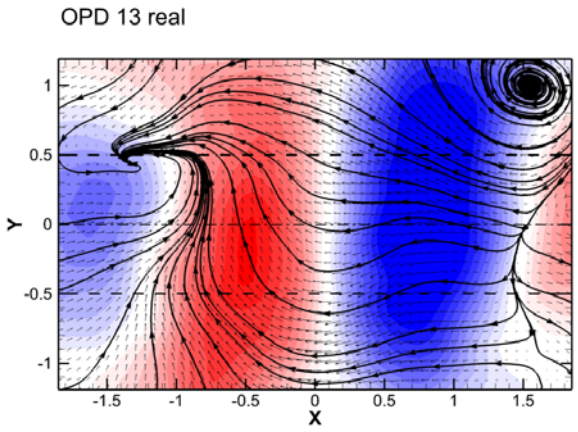

Fig. 10. Real part of the OPD mode 13 topology.

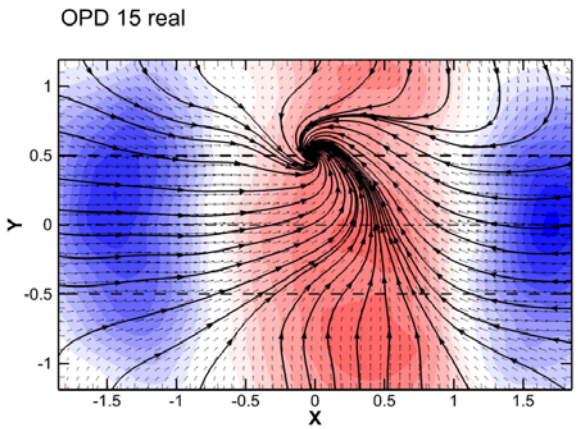

Fig. 11. Real part of the OPD mode 15 topology.

The last group of the OPD modes to be presented here are theses with the periodicity value around 0,1, the modes number 9, 10 and 11. Again, only real parts of the OPD modes are shown, the imaginary counter-parts are qualitatively similar, however the topology is shifted in space. The modes could be characterized by a couple of contra-rotating vortices accompanied with spots of positive and negative fluctuations of streamwise velocity component. The real parts of the OPD modes 9, 10 and 11 are shown in Figures 12, 13 and 14 respectively.

The rest of the OPD modes are characterized by strong decay in time and/or very low frequency. The modes 1-4 are characterized even by zero frequency, this means that those modes are not of cyclostationary nature, but only simply decaying in time, the topology is constant.

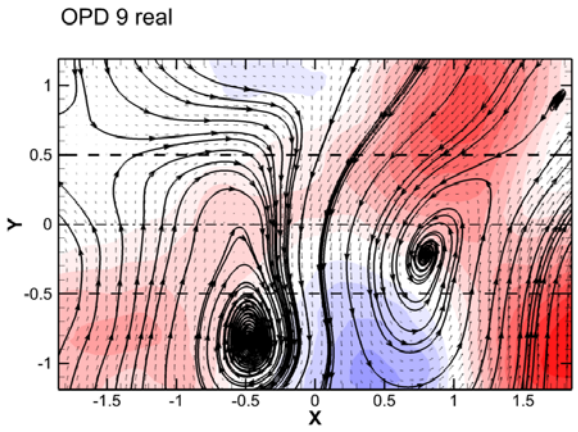

Fig. 12. Real part of the OPD mode 9 topology.

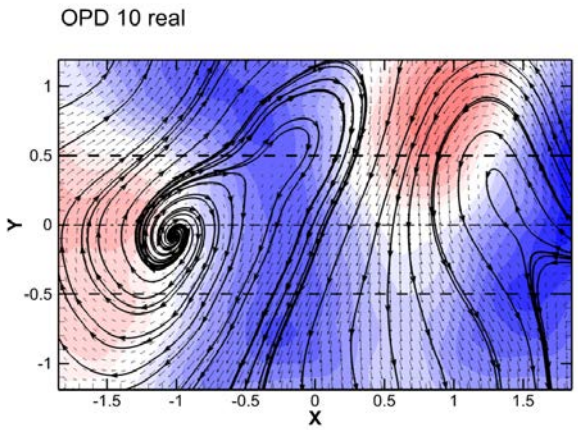

Fig. 13. Real part of the OPD mode 10 topology.

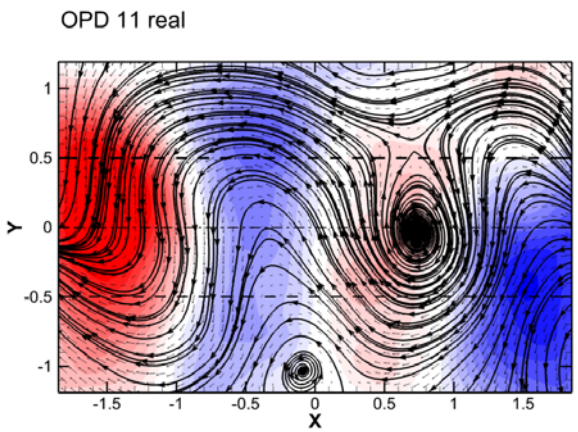

Fig. 14. Real part of the OPD mode 11 topology.

4 Conclusions

The flow in the wake behind prismatic circular cylinder could be considered to be 2D in sense of statistical characteristics, however instantaneous flow patterns are always 3D. The 3D dynamical structure of the wake was studied experimentally using stereo PIV time-resolved technique. The dynamical analysis of the acquired data was performed with help of the OPD method capturing decaying spatial harmonic oscillations, represented by the OPD modes.

The dominant OPD mode with the most stable oscillations characterizes the von Kármán vortex street existing within the wake, which is characterized by the same frequency. The mode topology could be described by oscillating shear layer across the cylinder axis and periodic appearance of the system contra-rotation streamwise vortices during one half of the period, then disappearing and reappearing again.

The remaining dynamical content represented by the other OPD modes is much more random in nature and weaker as for the amplitudes. The topology od modes corresponding to this behaviour could be characterized by system of streamwise vortices in combination with spotty pulsations of the streamwise velocity component.

This work was supported by the Grant Agency of the Czech Republic, project No. 17-01088S.

References

1. V. Uruba, On 3D Instability of Wake behind a Cylinder, AIP Conference Proceedings 1745 (1), 020062, (2016)
2. J. Hoffman, C. Johnson, Resolution of d'Alembert's paradox, *J. Math. Fluid Mech.*, **12** (3), pp.321-334, (2010)
3. C.H.K. Williamson, Vortex Dynamics in the Cylinder Wake, *Annu. Rev. Fluid. Mech.* (1996) **28** pp.477-539
4. V. Uruba, Decomposition methods in turbulent research, EFM11, *EPJ Web of Conferences*, **25** 01095 (2012)
5. V. Uruba, Near Wake Dynamics around a Vibrating Airfoil by Means of PIV and Oscillation Pattern Decomposition at Reynolds Number of 65 000, *Journal of Fluids and Structures*, **55**, pp. 372-383 (2015)
6. P. Procházka and V. Uruba, Reynolds Number Effect on Velocity Field and on Coherent Structures behind a Cylinder, AIP Conf. Proc. **2118**, 030037-1–030037-4; (2019)